過去十個月中(2009 年 8 月至 2010 年 5 月),本實驗室在國科會經費支持下對鐵-(20~25) at.%鋁-(6~9) at.%鈦合金的相變化進行研究，並已將其中部分研究成果整理成論文發表，其餘研究成果也正在整理準備發表中。較重要的成果為：鐵-20 at%鋁-8 at%鈦合金固溶處理後的顯微結構為 A2+D03 雙相,當此固溶合金作時效熱處理,其溫度範圍為 750˚C 到 1100˚C,可發現隨時效熱處理溫度增加時,此固溶合金的相轉變過程依序為 A2+D03→A2+D03+C14→B2+C14→A2+C14→A2,此相變化過程從未在鐵鋁鈦合金研究過程中被發現過。這部分的研究結果我們正在整理中，即將寫成論文" Phase transformations in an Fe-20 at.% Al-8 at.% Ti alloy " 投稿至期刊 Scripta Materialia。接下來除舉出我們正在進行投稿作業之論文外，另列出本研究群正執行中之數項技術轉移案、及已獲通過或正申請中的專利，本篇期中精簡報告內容則為本研究群對 Fe-20 at.% Al-8 at.% Ti 合金之研究成果。

一、論文：

1. 期刊名稱：Scripta Materialia (2009 Impact factor: 2.887)
   計畫編號：NSC97-2221-E009-027-MY3
   著作內容：K.M. Chang, C.W. Su, G.D. Tsay, C.G. Chao and T.F. Liu, " Phase transformations in an Fe-20 at.% Al-8 at.% Ti alloy", submitted to Scripta Materialia (2010)

二、技術轉移案：

(1) 鐵鋁錳碳合金高爾夫球頭精密鑄造、鍛造和鑄鍛系列產品（復盛、明安、鉅明等三家公司，2005~2010）

(2) 刀削式鰭片散熱器、刀具及其加工法（聚亨公司，2003~2009）

三、專利：

(1) 低密度高強度高韌性合金材料及其製法（High Strength and High Toughness Alloy with Low Density and The Method of Making）（2007~2025，中華民國專利 I279448 號、美國專利 20070084528 公告中、日本專利正在審核中）

(2) 刀削式鰭片散熱器、刀具及其加工法（2003~2018，中華民國專利 511449 號）

(3) 低密度高韌性合金材料及其製法（Low Density And High Toughness Alloy And The Process For Making Same）（中華民國、美國、日本專利申請中）

(4) 低密度合金材料及其製法（Low Density Alloy And The Method of Making）（中華民國、美國、日本專利申請中）

Phase transformations in an Fe-20 at.% Al-8 at.% Ti alloy

C.W. Su, G.D. Tsay , Y.H. Tuan, C.L. Lin, K.M. Chang, P.C. Chen, H.Y. Wang, C. Y. Chen, C.Y. Lin and T.F. Liu*
Department of Materials Science and Engineering, National Chiao Tung University,
(NSC 97-2221-E-009-027-MY3)

Abstract

As-quenched microstructure of the Fe-20 at.% Al-8 at.% Ti alloy was a mixture of (A2+$D0_3$) phases. When the as-quenched alloy was aged at temperatures ranging from 750˚C to 1100˚C, the phase transition sequence as the aging temperature increased was found to be A2+$D0_3$→A2+$D0_3$+C14→B2+C14→A2+C14→A2. It is noted here that this phase transition has never been observed by other workers in the Fe-Al-Ti alloys before.

Keywords: iron aluminum titanium alloys, Phase transformations, transmission electron microscopy, phase separation.

1. Introduction

Efforts to improve the strength of Fe-Al alloy systems at elevated temperatures have been looked for by many workers from the point of the critical temperature T_c for the $D0_3$→B2 transition [1-6]. One of them is the addition of Ti alloying element on the Fe-Al binary alloys [4-6]. According to their reports, the effect of Ti addition on the Fe-Al alloy systems not only increased the $D0_3$→B2→A2 transition temperatures, but also expanded the (A2+ $D0_3$) phase region of the Fe-Al alloy systems. In other word, the limited stability of the $D0_3$ structure can be raised from about 550˚C for binary Fe-Al alloys with 25 at.% Al to approximate 825˚C for adding 5 at.% Ti on the Fe_3Al alloy [6]. As a result, a significant increase in the strength and hardness of Fe-Al-Ti alloys at elevated temperatures was eventually achieved by raising the critical temperature T_c of $D0_3$→B2 transition. In addition, some investigators pointed out that the strength could also be improved due to the precipitation of the hexagonal Fe_2Ti with C14 phase [7-9]. Previous studies have shown that when Ti content increased greater than 7 at.%, the C14 phase could start to precipitate at grain boundaries and within grains [10].

In the previous studies [6], it is clearly seen that although the phase transformations in the Fe-Al-Ti alloys have been studied, most of the examinations were only focused on the Fe-Al-Ti alloys with lower Ti content. Information concerning the microstructural development of the Fe-Al-Ti alloys with higher Ti content is very insufficient. Therefore, the purpose of the present study is to investigate the as-quenched microstructures of the Fe-Al-Ti alloys with Ti > 7 at.%.

2. Experimental Procedure

The Fe-20 at.% Al-8 at.% Ti alloy was prepared in a vacuum induction furnace by using high purity (99.99%) constituent elements. After being homogenized at 1250˚C for 48 h, the ingot was sectioned into 2-mm-thick slices. These slices were subsequently solution heat-treated at 1250˚C for 1 h and then rapidly quenched into room-temperature water. The aging processes were performed at temperatures ranging from 750˚C to 1100˚C in a vacuum heat-treated furnace for various times and then quenched into room-temperature water rapidly. TEM specimens were prepared by means of double-jet electropolisher with an electrolyte of 67% methanol and 33% nitric acid. TEM observation of microstructure was performed on a JEOL JEM-2000FX TEM operating at 200kV. This microscope was equipped with a Link ISIS 300 energy-dispersive X-ray spectrometer (EDS) for chemical analysis. Quantitative analyses of elemental concentrations were made with a Cliff-Lorimer Ratio Thin Section method.

3. Results and Discussion

Figure 6.1(a) is a bright-field (BF) electron micrograph of the as-quenched alloy. Figure 6.1(b) is a selected-area diffraction pattern (SADP) of the as-quenched alloy, exhibiting the superlattice reflection spots of the ordered $D0_3$ phase [11]. Figure 6.1(c) is a $(\bar{1}11)$ $D0_3$ dark-field (DF) electron micrograph of the as-quenched alloy, revealing the presence of extremely fine $D0_3$ domains. Figure 6.1(d), a (002) $D0_3$ DF electron micrograph, shows the presence of small B2 domains with a/4<111> APBs. Since the sizes of both $D0_3$ and B2 domains are very small, it is suggested that these domains were formed by ordering transition during quenching. In Figure 6.1(d), it is also seen that a very high density of disordered A2 phase (dark contrast) was present within the B2 domains. It is concluded from the above observations that in the as-quenched condition, the microstructure of the alloy was a mixture of (A2+$D0_3$) phases, which were formed by an A2→B2→(A2+$D0_3$) ordering transition during quenching [12-19]. This result is similar to that observed by other workers in the Fe-(18~22.5) at.% Al-5 at.% Ti alloys [6].When the as-quenched alloy was aged at 750˚C, the $D0_3$ domains grew, as illustrated in Figure 6.2. Figure 6.2 is a DF electron micrograph obtained by use of the (200) superlattice reflection in [001] zone, revealing that the $D0_3$ domains were formed lying along <100> directions. This feature is also similar to that observed by Mendiratta *et al.* in the aged Fe-Al-Ti alloys [6]. With increasing the aging time at 750˚C, the $D0_3$ domains continued to grow and the morphology changed from cubic to granular shape, as illustrated in Figure 6.3. Figures 6.3(a) and (b) are $(\bar{1}11)$ and (002) $D0_3$ DF electron micrographs, clearly showing that the $(\bar{1}11)$ and (002) $D0_3$ DF are morphologically identical. Since the (002) reflection spot comes from both the B2 and $D0_3$ phases, while the $(\bar{1}11)$ reflection spot comes only from $D0_3$ phase,

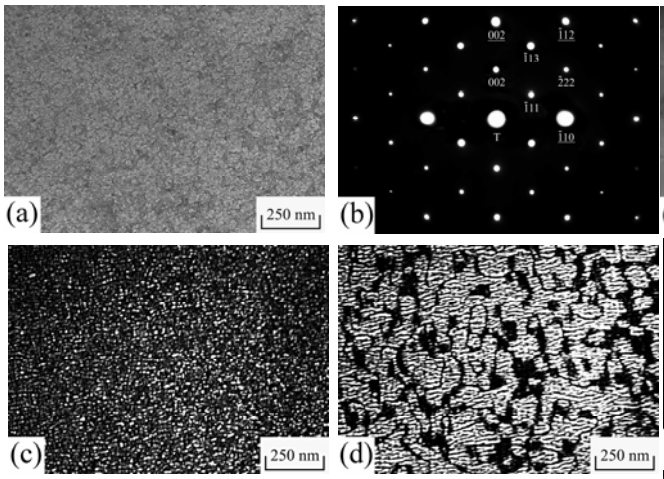

Figure 6.1 Electron micrographs of the as-quenched alloy: (a) BF, (b) an SADP. The foil normal is [110]. (hkl = ferrite phase; hkl = $D0_3$ phase.), (c) and (d) $(\bar{1}11)$ and (002) $D0_3$ DF, respectively.

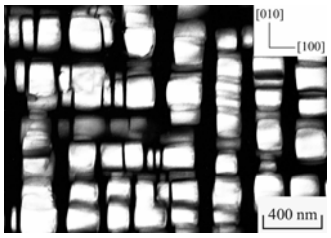

Figure 6.2 (200) $D0_3$ DF electron micrograph of the alloy aged at 750˚C for 1 h.

the bright particles presented in Figures 6.3(a) and (b) are considered to be $D0_3$ phase, not B2 phase. This result indicates that the microstructure of the alloy present at 750˚C was a mixture of (A2+$D0_3$) phases. Figure 6.4(a) is a bright-field (BF) electron micrograph of the alloy aged at 850˚C for 1 h. In this figure, it is clear that some rod-like precipitates were found to appear within the matrix. Figures 6.4(b) through (d) demonstrate three different SADPs taken from an area including the precipitate marked as "C" in Figure 6.4(a) and its surrounding matrix. The crystallographic normals of the (A2+$D0_3$) matrix are $[1\,1\,1]_m$, $[1\,1\,0]_m$ and $[\bar{1}\,\bar{1}\,2]_m$, respectively. In addition to the reflection spots corresponding to the (A2+$D0_3$) phases, the diffraction patterns also consist of small spots caused by the presence of the precipitate. According to the camera length and the measurement of angles as well as d-spacings of the diffraction spots, the crystal structure of the precipitate phase was determined to be hexagonal with lattice parameters a=0.505 nm and c=0.801

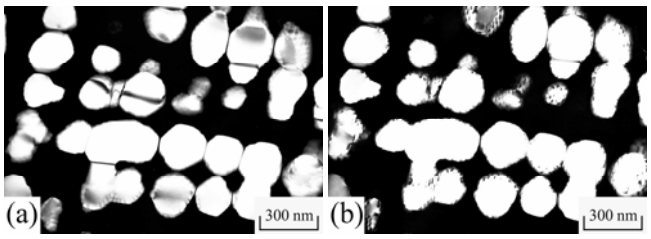

Figure 6.3 Electron micrographs of the alloy aged at 750˚C for 12 h: (a) and (b) $(\bar{1}11)$ and (002) $D0_3$ DF, respectively.

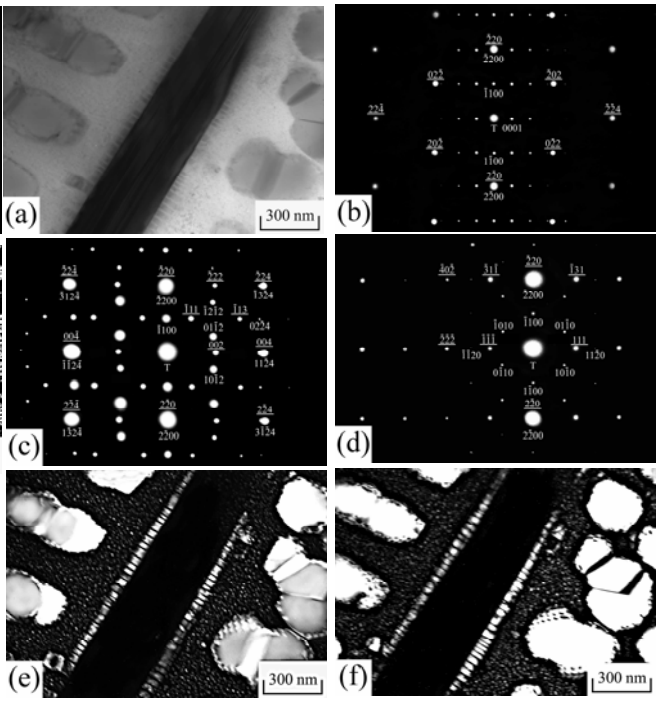

Figure 6.4 Electron micrographs of the alloy aged at 850˚C for 1 h: (a) BF, (b) through (d) three SADPs taken from an area including the C14 precipitate and its surrounding matrix. The zone axes of the (A2+$D0_3$) matrix are (b) [1 1 1], (c) [1 1 0], (d) $[\bar{1}\,\bar{1}\,2]$, respectively. (hkil = C14 precipitate; hkl = $D0_3$ phase), (e) and (f) $(\bar{1}11)$and $(002)$$D0_3$ DF, respectively.

nm, which corresponds to that of the C14 phase [20]. Analyses by the above diffraction patterns, the orientation relationship between the C14 precipitate and (A2+$D0_3$) matrix was determined to be $(0\,0\,0\,1)_{C14}//(\bar{1}\,\bar{1}\,2)_m$, $(\bar{1}\,1\,0\,0)_{C14}//(\bar{1}\,1\,0)_m$, $(1\,1\,\bar{2}\,0)_{C14}//(1\,1\,1)_m$. It is worthy mentioning that the orientation relationship between the C14 precipitate and A2, $D0_3$ or B2 matrix has never been reported by other workers in the Fe-Al-Ti alloy systems before. Figures 6.4(e) and (f) are $(\bar{1}11)$ and (002) $D0_3$ DF electron micrographs, clearly revealing that three types of $D0_3$ particles could be detected: one is the granular-like $D0_3$ particles within the matrix; another is the cuboidal $D0_3$ particles contiguous to the C14 precipitate. Since the sizes of these two types of $D0_3$ particles are larger than those observed in the as-quenched alloy. It is therefore reasonable to believe that these two types of the $D0_3$ particles were existent at the aging temperature. The other is the extremely fine $D0_3$ particles within the A2 matrix, which were formed during quenching. It is concluded from the above observations that the microstructure of the alloy present at 850˚C was a mixture of (A2+$D0_3$+C14). Shown in Figure 6.5(a) is $(\bar{1}11)$ $D0_3$ DF electron micrograph of the alloy aged at 900˚C for 1 h and then quenched. It reveals that the extremely fine $D0_3$ domains with a/2<100> APBs could be observed. The size of the $D0_3$ domains is very small, indicating that the extremely fine $D0_3$ domains were formed during quenching from the aging temperature; otherwise, its size should be increased at the aging temperature. Figure 6.5(b), a (002) $D0_3$ DF electron micrograph of the same area as Figure 6.5(a), shows that along with growth of the B2 domains, the a/4<111> APBs had gradually disappeared. Furthermore, it is also seen that the disordered A2 phase with a dark contrast could be

observed within the B2 domains. This indicates that the matrix present at 900˚C should be B2 phase and the extremely fine $D0_3$ domains were formed by a B2→(A2+$D0_3$) ordering transition during quenching. Accordingly, the microstructure of the present alloy at 900˚C was a mixture of (B2+C14) phases. However, when the alloy was aging at 950˚C for 1 h and then quenched, the $(\bar{1}11)$ and (002) $D0_3$ DF electron micrographs revealed that in addition to C14 precipitates, only quenched-in extremely fine $D0_3$ domains and small B2 domains were present within the matrix. An example is illustrated in Figure 6.6. This means that the stable microstructure of the present alloy at 950˚C was a mixture of (A2+C14) phases.

Progressively higher temperature aging and quenching experiments indicated the mixture of (A2+C14) phases could be preserved up to 1050˚C. However, when the alloy was aged at 1100˚C and then quenched, the C14 precipitates disappeared and only quenched-in small B2 domains (the size being comparable to that observed in the as-quenched alloy) could be detected, as illustrated in Figure 6.7. This indicates that the microstructure of the present alloy existing at 1100˚C or above should be the single disordered A2 phase. It is therefore concluded that with increasing the aging temperature from 750˚C to 1100˚C, the phase transition sequence in the present alloy was A2+$D0_3$→A2+$D0_3$+C14→B2 +C14→A2+C14→A2.

Based on the above observations, two important features of the present study are worthy to note as follows: (I) When the present alloy was aged at 850˚C, the cuboidal $D0_3$ particles could be observed to form contiguous to the C14 precipitates. It is a remarkable feature in the present study, which has never been observed by others in the Fe-Al-Ti alloy systems before. In order to clarify this feature, an STEM-EDS study was made. Figures 6.8(a) through (d) represent four typical EDS spectra taken from a granular-like $D0_3$ particle within the matrix, a cuboidal $D0_3$ particle contiguous to the C14 precipitate, C14 precipitate and the (A2+$D0_3$) matrix in the alloy aged at 850˚C for 1h, respectively. The average concentrations of alloying

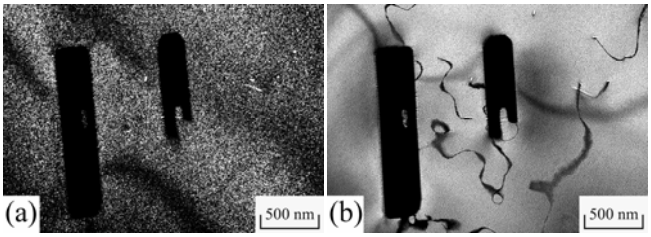

Figure 6.5 Electron micrographs of the alloy aged at 900˚C for 1 h: (a) and (b) $(\bar{1}11)$ and (002) $D0_3$ DF, respectively.

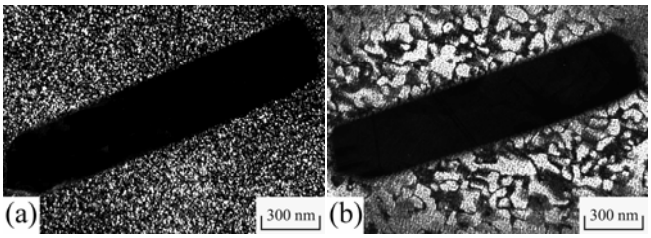

Figure 6.6 Electron micrographs of the alloy aged at 950˚C for 1 h: (a) and (b) $(\bar{1}11)$ and (002) $D0_3$ DF, respectively.

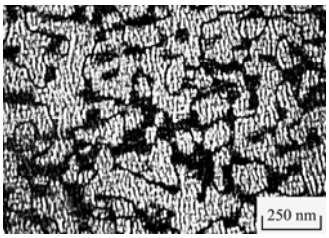

Figure 6.7 (002) $D0_3$ DF electron micrograph of the alloy aged at 1100˚C for 1 h.

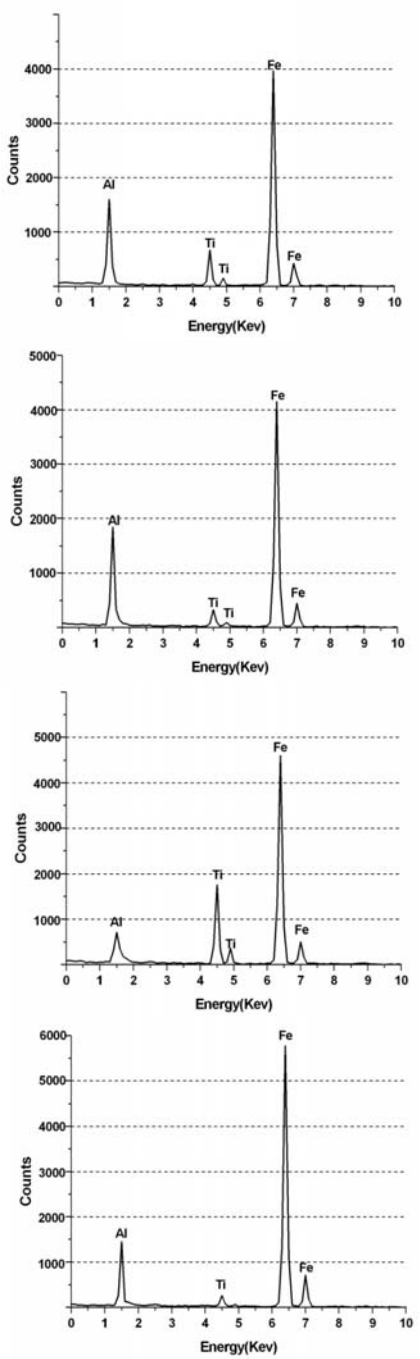

Figure 6.8 (a) through (d) four typical EDS spectra taken from a granular-like $D0_3$ particle within the matrix, a cuboidal $D0_3$ particle contiguous to the C14 precipitate, C14 precipitate and the (A2+$D0_3$) matrix in the alloy aged at 850˚C for 1 hour, respectively.

elements obtained by analyzing a number of EDS spectra of each phase are listed in Table 6.1. For comparison, the chemical compositions of the as-quenched alloy are also listed in Table 6.1. The quantitative analyses revealed that the atomic percentages of the alloying elements in the C14 precipitate and cuboidal $D0_3$ particle were Fe-9.4at.% Al-25.7 at.% Ti and Fe-25.9 at.% Al-6.3 at.% Ti. It is clear that the concentration of Ti in the C14 precipitate is much higher than that in the as-quenched alloy and the concentration of Al is obviously lower than that in the as-quenched alloy. However, it is seen in Figure 6.8(b) and Table 6.1 that Al concentration in the cuboidal $D0_3$ particles is much higher than C14 precipitate and ($A2+D0_3$) matrix. Therefore, it is expected that along with the precipitation of C14 phase, the surrounding regions would be enriched in Al. The enrichment in Al would cause the Al-rich $D0_3$ particles to form at the regions contiguous to the C14 precipitates, as observed in Figure 6.4(e). (Ⅱ) It is well-known that the $D0_3$ phase could be formed by ordering transition during quenching with Al > 20 at.% in the Fe-Al binary alloys [13]. However, it is clear in Figure 6.4(e) that the $A2 \rightarrow A2+D0_3$ ordering transition could be detected and the Al content in the A2 phase was examined to be 17.9 at.% only. Therefore, it is believed that the solubility of 4.9 at.% Ti within the A2 phase would enhance the $A2 \rightarrow A2+D0_3$ ordering transition to occur during quenching. (Ⅲ) Recently, Morris *et al.*, reported that when the Fe-25 at.% Al-2 at.% Nb alloy was aged at 800˚C, C14 precipitates were formed within the $D0_3$ matrix and the orientation relationship between the C14 precipitate and $D0_3$ matrix was $\{\bar{1}\,0\,1\,0\}_{C14}//\{\bar{1}\,0\,1\}_m$, $<1\,\bar{2}\,1\,0>_{C14} \approx <010>_m$ and $<0\,0\,0\,1>_{C14} \approx <101>_m$ [21]. Accordingly, Morris *et al.* claimed that the only exact relationship was $\{\bar{1}\,0\,1\,0\}_{C14}//\{\bar{1}\,0\,1\}_m$ and all other relationships were approximate with a difference of a few degrees (3~5˚). Compared with present work, it is worthy to note here that only $(\bar{1}\,1\,0\,0)_{C14}//(\bar{1}\,1\,0)_m$ is indeed in agreement with Morris *et al.*, but the other relationships are discrepant.

Table 6.1 Chemical Compositions of the Phases Revealed by Energy-Dispersive X-ray Spectrometer (EDS)

Heat Treatment	Phase	Chemical Compositions (at.%)		
		Fe	Al	Ti
as-quenched	$A2+D0_3$	71.7	20.2	8.1
850°C, 1 h	granular-like $D0_3$	65.4	23.2	11.4
	cuboidal $D0_3$	67.8	25.9	6.3
	C14	64.9	9.4	25.7
	$A2+D0_3$	77.2	17.9	4.9

4. Conclusion

(1) The as-quenched microstructure of the Fe-20 at.% Al-8 at.% Ti alloy was a mixture of ($A2+D0_3$) phases. The ($A2+D0_3$) phases were formed by an $A2 \rightarrow B2 \rightarrow (A2+D0_3)$ ordering transition during quenching.

(2) When the alloy was aged at 750˚C, the $D0_3$ precipitates grew lying along <100> directions. With increasing aging time, the $D0_3$ domains continued to grow and the morphology changed from cuboidal to granular shape.

(3) When the alloy was aged at 850˚C for 1 h, the rod-like C14 precipitates could be observed within the ($A2+D0_3$) matrix. Along with the growth of the C14 precipitates, the surrounding region would be enriched in aluminum. The enrichment of aluminum would enhance the formation of the cuboidal $D0_3$ particles at the regions contiguous to the C14 precipitates.

(4) When the as-**q**uenched alloy was aged at temperatures ranging from 750˚C to 1100˚C, the phase transformation sequence as the aging temperature increased was found to be ($A2+D0_3$) → ($A2+D0_3$+C14) → (B2+C14) → (A2+C14) → A2.

(5) The orientation relationship between the C14 precipitate and ($A2+D0_3$) matrix was determined to be $(0\,0\,0\,1)_{C14}//(\bar{1}\,\bar{1}\,2)_m$, $(\bar{1}\,1\,0\,0)_{C14}//(\bar{1}\,1\,0)_m$, $(1\,1\,\bar{2}\,0)_{C14}//(1\,1\,1)_m$, which has never been reported in the Fe-Al-Ti alloy systems before.

Acknowledgements

The authors gratefully acknowledge the financial support for this research by the National Science Council of the Republic of China under contract no. NSC 97-2221-E-009-027-MY3.

References

1. J. M. Cairney, P. R. Munroe, J. Mater. Sci. Letters 18 (1999) 449.
2. U. Prakash, R.A. Buckley, H. Jones, Mater. Sci. Tech. 9 (1993) 16.
3. Y. Nishino, S. Asano, T. Ogawa, Mater. Sci. Eng. A 234-236 (1997) 271.
4. L. Anthony, B. Fultz, Acta metall. mater. 43 (1995) 3885.
5. Y. Nishino, C. Kumada, S. Asano, Scripta Mater. 36 (1997) 461.
6. M.G. Mediratta, S.K. Ehlers, H.A. Lipsitt, Metall. Trans. A 18 (1987) 509.
7. M. Palm, Intermetallics 13 (2005) 1286.
8. F. Stein, M. Plam, G. Sauthoff, Intermetallics 13 (2005) 1056.
9. F. Stein, M. Plam, G. Sauthoff, Intermetallics 13 (2004) 713.
10. C.H. Sellers, T.A. Hyde, T.K. O'Brien, R.N. Wright, J. Phys. Chem. Solids 55 (1994) 505.
11. C.H. Chen, T.F. Liu, Metall. Trans. A 34 (2003) 503.
12. S.M. Allen and J.W. Cahn: Acta Mater. 24 (1976) 425-437.
13. P.R. Swann, W.R. Duff and R.M. Fisher: Metall. Trans. 3 (1972) 409-419.
14. C.H. Chen and T.F. Liu: Scripta Mater. 47 (2002) 515-520.
15. S.Y. Yang and T.F. Liu: Scripta Mater. 54 (2006) 931-935.
16. T.F. Liu, J.S. Chou and C.C. Wu: Metall. Trans. A 21 (1990) 1891-1899.
17. S.Y. Yang and T.F. Liu: J. Alloys Compd. 417 (2006) 63-68.
18. M. Palm, G. Inden, N. Thomas, J. Phase Equilibria 16 (1995) 209.
19. D.G. Morris, L.M. Requejo, M.A. Muñoz-Morris, Intermetallics 13 (2005) 862.